A geometric parameterization for beta turns

Nicholas E. Newell, Independent Researcher, 21 Parkview Rd., Reading MA 01867 USA
nenewell@comcast.net

Abstract

Beta turns, in which the protein backbone abruptly changes direction over four amino acid residues, are the most common type of protein secondary structure after helices and strands and play key structural and functional roles. Previous work has produced classification systems for turn backbone geometry at multiple levels of precision, but these operate in the Ramachandran space of backbone dihedral angles, and the absence of a local Euclidean-space coordinate system and structural alignment for turns, or of any systematic Euclidean-space characterization of turn backbone shape, presents challenges for the visualization, comparison and analysis of the wide range of turn conformations and the design of turns and the structures that incorporate them. This work derives a local coordinate system that implicitly aligns beta turns, together with a simple geometric parameterization for turn backbone shape that describes modes of structural variation not explicitly captured by existing systems. These modes are shown to be meaningful by the demonstration of clear relationships between parameter values and the electrostatic energy of the common beta-turn H-bond, the overrepresentation of key side-chain motifs, and the structural contexts in which turns are found. Geometric turn parameters, which complement existing Ramachandran-space classifications, can be used to select structures for compatibility with particular side-chain interactions or contexts, and they should prove valuable in applications, such as protein design, where an enhanced Euclidean-space description of turns may improve understanding or performance. The web-based tools ExploreTurns, MapTurns and ProfileTurn, available at www.betaturn.com, incorporate turn-local coordinates and turn parameters and demonstrate their utility.

Keywords

Beta turn, beta-bulge loop, beta hairpin, protein structure, secondary structure, structural analysis, structural bioinformatics, protein design, hydrogen bond, sequence motif

Abbreviations

AA: Amino acid

BB: Protein backbone

SC: Amino acid side-chain

Turn position index: Specifies residue positions in the turn and its four-residue N-/C-terminal BB neighborhoods according to the key: -4-3-2-1<1234>+1+2+3+4, where the brackets delineate the turn.

MCN + position index: Main-chain NH-group H-bond donor at the specified position. For example, MCN-1, MCN2, and MCN+3 refer to the BB H-bond donors one residue before the turn, at the second turn residue, and three residues after the turn respectively.

MCO + position index: Main-chain carbonyl oxygen H-bond receptor at the specified position.

BB H-bonds: BB H-bonds are specified by indicating the donor and acceptor positions in the turn frame, separated by '>'. For example, "4>-1" specifies an H-bond donated by MCN4 and accepted by MCO-1.

AA sequence motifs: AA sequence motifs in a turn or its BB neighborhood are labelled with the single-letter codes of the included AAs, each followed by its position index. For example, "D-1T3" specifies Asp just before the turn and Thr at the third turn position.

PDB addresses: PDB addresses for turn structures are given in the format ABCD_X_N, where ABCD is the 4-character PDB file name, X is the chain letter, and N is the position in the chain of the first turn residue.

BBL: Beta-bulge loop; also BBL1 (type 1), BBL2 (type 2).

1 | Introduction

1.1 Background

Abrupt changes in the direction of the protein backbone (BB) chain are accomplished by tight turns of types π, α, β, γ, and δ, with lengths of 6, 5, 4, 3, and 2 amino acid (AA) residues respectively[1]. Of these types, the four-residue beta turn is found most frequently; it constitutes the third most common protein secondary structure after alpha helices and beta strands. Either individually or in overlapping multiples[2], beta turns are found in the loops between segments of repetitive BB structure, and they are also very common in extended loops.

Beta turns were first described in 1968 by Venkatachalam[3], who determined the allowed geometries of four-residue chain segments that exhibit a 4>1 H-bond. Since this study, a substantial body of analytical work (see brief review in[4]) has evolved the beta-turn definition and identified and classified new geometries. A current definition[4], applied here, specifies a four-residue BB segment in which the distance between the alpha carbons of the first and last residues is no greater than 7Å and the two central residues are not part of helices or strands. In about half of the segments that meet this definition, the BB NH group of the fourth turn residue (MCN4) donates an H-bond to the BB carbonyl oxygen of the first residue (MCO1), and the presence of this 4>1 H-bond by itself constitutes an alternative, more restrictive definition.

Three beta-turn classification systems developed in previous studies are employed in this work; each partitions turns by BB geometry in Ramachandran space at a different level of precision. These systems, described in the ExploreTurns[5] online help, are referred to here, in order of increasing precision, as the "classical" type system, finalized by Hutchinson and Thornton[6], and the BB cluster and Ramachandran type systems, both derived by Shapovalov et al.[4], with the last system based on the map of Ramachandran space due to Hollingsworth and Karplus[7]. Beta turns exhibit a wide range of BB conformations which, taken together with the variety of intra- and extra-turn structural interactions that their side-chains (SCs) can mediate, enable them to play crucial roles in multiple contexts; for an overview, see *Roles of beta turns in proteins* at www.betaturn.com.

1.2 Motivation and description of the present work

The inherent difficulty of visualizing and contrasting the wide range of beta-turn geometries in Ramachandran space motivated the construction of a turn-local coordinate system which could provide a common Euclidean-space framework for

structural analysis, and the derivation of geometric parameters for turns was suggested by the observation that while the shape of a protein helix, which can be described as a series of overlapping turns, has been characterized by parameters such as twist, rise, and pitch that vary between helix types and also with the irregularities of helices within each type[8], no such parameterization had been developed to describe the bulk BB shapes of beta turns, which vary between and within turn types or BB clusters.

A turn-local coordinate system with geometric parameters complements Ramachandran-space turn classification systems, enabling a meaningful discrimination of structure within types and clusters. The potential utility of geometric parameters as structural discriminators is highlighted by the fact that the set of turns with both central residues in or near the right-handed helical conformation, which constitutes close to half of all turns, is represented by a single classical type (I) and a single BB cluster (with Ramachandran-type label AD)[4], yet, as shown below, type I/cluster AD includes a range of conformations which are compatible to widely varying degrees with key SC motifs, or compatible with different SC motifs entirely, and play distinct roles in the structural contexts that incorporate beta turns. The presence of a meaningful range of BB structures within type I/cluster AD, and also, to varying degrees, within other, smaller types/clusters, prompted a search for a set of parameters capable of characterizing modes of geometric variation not explicitly captured by Ramachandran-space systems.

The construction of a turn-local coordinate system is achieved via a set of geometric definitions, and the representation of turns in the local system implicitly aligns them. Using the definitions, the turn parameters are then derived, their modes of variation are demonstrated with example structures, and their distributions within each classical type and BB cluster are plotted. Parameter distributions are also heat-mapped across the Ramachandran-angle spaces of the two central turn residues, revealing the key bond rotations that drive parameter variation in each type or cluster.

The fractional overrepresentation of key sequence motifs in turns is shown to vary dramatically with parameter values, demonstrating the utility of parameters as structural discriminators that can support geometric tuning for compatibility with SC interactions, and relationships are also demonstrated between parameter values and the electrostatic energy of the 4>1 H-bond.

The roles and contexts of parameter regimes are explored, as are the relationships between *cis*-peptide bonds and parameter values. The dependencies between parameters are also evaluated, and the potential utility of parameters for structure validation is explored.

Many of the results presented here were generated with ExploreTurns[5], a facility for the comprehensive exploration, analysis, geometric tuning and retrieval of beta

turns and their contexts from the dataset compiled for this study. A second tool, MapTurns[9], produces interactive, 3D conformational heatmaps of the BB and SC structure, H-bonding and contexts associated with sequence motifs in beta turns, and a third tool, ProfileTurn, profiles a turn uploaded by the user and evaluates the compatibility between its geometry and motif content. Extensive online support is available within all three tools, which are available at www.betaturn.com.

2 | Methods

2.1 Euclidean-space representation and alignment

The derivation of turn parameters begins with a set of geometric definitions which establish a common turn-local Euclidean-space coordinate system. The **span line** is the line between a turn's first and last alpha carbons ($C_{\alpha 1}$and $C_{\alpha 4}$), and the span, already used in the beta-turn definition, is its length. The **turn center** is the midpoint of ($C_2 \rightarrow N_3$), the middle peptide bond in the turn. The **turn plane** contains the span line and passes through the turn center, and the perpendicular dropped from the turn center to the span line defines the **turn axis**. Using these definitions, a local orthogonal right-handed coordinate system is established. The system's origin lies at the turn center, while the x axis lies in the turn plane, collinear with the turn axis, with its positive sense oriented from the center towards the span line. The y axis lies in the turn plane, parallel to the turn span, with its positive sense oriented towards the C-terminal half of the turn, and finally the z axis is perpendicular to the turn plane, with its positive sense determined by the cross-product of the x and y axes. For a depiction of the turn coordinate system, see any figure below that displays a structure.

The atomic coordinates of each turn are transformed from the global protein system in the turn's PDB[10] file to the turn-local system, implicitly aligning the structures. The accuracy of this alignment is tested by a comparison between the implicit pairwise turn alignments and the best alignments generated by a perturbative search procedure (section 1.1 in Supplementary Material).

2.2 Parameter definitions

Span

The pre-existing span parameter measures the distance (Å) between $C_{\alpha 1}$ and $C_{\alpha 4}$, and a 7Å threshold for this parameter is part of the beta-turn definition. Two new span-related parameters are defined: the N- and C-terminal half-spans measure the distances between the turn axis and $C_{\alpha 1}$ and $C_{\alpha 4}$ respectively, and quantify the separate "widths"

of the N- and C-terminal halves of the turn, providing an additional degree of freedom in the measurement of span. Span values in the dataset range from a minimum of 3.13Å to the 7Å limit set by the beta-turn definition, while the N-terminal half-span ranges from 0 to 4.76Å, and the C-terminal half-span ranges from .76Å to 4.82Å.

Bulge

Bulge is a measure of the magnitude of the excursion in the turn plane that the beta-turn BB makes from the span line as it bends to form the turn. Bulge is defined as the distance (Å) from the turn center to the span line. Bulge values in the dataset range from 1.28Å to 4.7Å.

Skew

Skew is a dimensionless measure of the asymmetry of the projection of a beta turn's BB onto the turn plane. Skew is defined as the directed displacement along the span line between the line's center and the point of intersection between the turn axis and the line, divided by half the span. Skew is negative when the turn axis intersects the span line in its N-terminal half, indicating a "lean" towards the N-terminus, or positive when the axis intersects the line in its C-terminal half, producing a C-terminal lean. Skew is expressed in terms of the half-spans as:

$$skew = \frac{2S_N}{S_N + S_C} - 1 \qquad (1)$$

where S_N and S_C are the N- and C-terminal half-spans. Skew is therefore positive when S_N is larger than S_C, negative when the reverse is true, or zero when the half-spans are equal. A turn that skews so strongly N-terminally that its axis intersects the span line at the position of $C_{\alpha 1}$ (S_N = 0) would exhibit a skew of -1, while a turn skewed so strongly C-terminally that its axis intersects the line at $C_{\alpha 4}$ (S_C = 0) would show a skew of +1. Skew values in the dataset range from -1 to .78.

Warp

Warp measures the departure from flatness of a beta turn's BB in the z dimension of the turn coordinate system, perpendicular to the turn plane. Warp (Å) is defined as the average absolute excursion of the turn's BB above or below the turn plane between $C_{\alpha 1}$ and $C_{\alpha 4}$, excluding BB carbonyl oxygen atoms as well as $C_{\alpha 1}$ and $C_{\alpha 4}$ themselves (since they lie within the plane). The eight BB atoms used to compute warp are therefore (C_1, N_2, $C\alpha_2$, C_2, N_3, $C\alpha_3$, C_3, N_4). Warp values in the dataset range from .14Å to 1.25Å. The differences in BB geometry between turn types or BB clusters affects the

interpretation and utility of the warp parameter (section 3.1 in Supplementary Material).

2.3 Other methods

Sections 1.2 and 1.3 in Supplementary Material describe the redundancy-screened beta-turn dataset of 102,192 turns and the H-bond definition. The statistical methods used to calculate the overrepresentation of sequence motifs[11,12,13] are described in the ExploreTurns user guide at www.betaturn.com.

3 | Results

3.1 Parameter ranges in structures

Figure 1 shows examples of turns with parameter values near the limits of span, bulge, skew and warp in the dataset.

3.2 Parameter distributions

Figure 2 plots the distributions of span, bulge, warp and skew in the classical types, while distributions for the BB clusters are given in section 2.1 in Supplementary Material. See the figure captions for brief comparative discussions of the distributions, as well as discussions of the partitioning of the distributions in the classical types into those of the BB clusters. Mean and mode parameter values in the BB clusters can be more extreme than those in any classical type; for example, the warp distribution for cluster AG_9 falls to the right of that of any type (Figure S1d), while cluster *cis*DP_18 shows average (negative) skew more than twice as great as any type (Figure S2c).

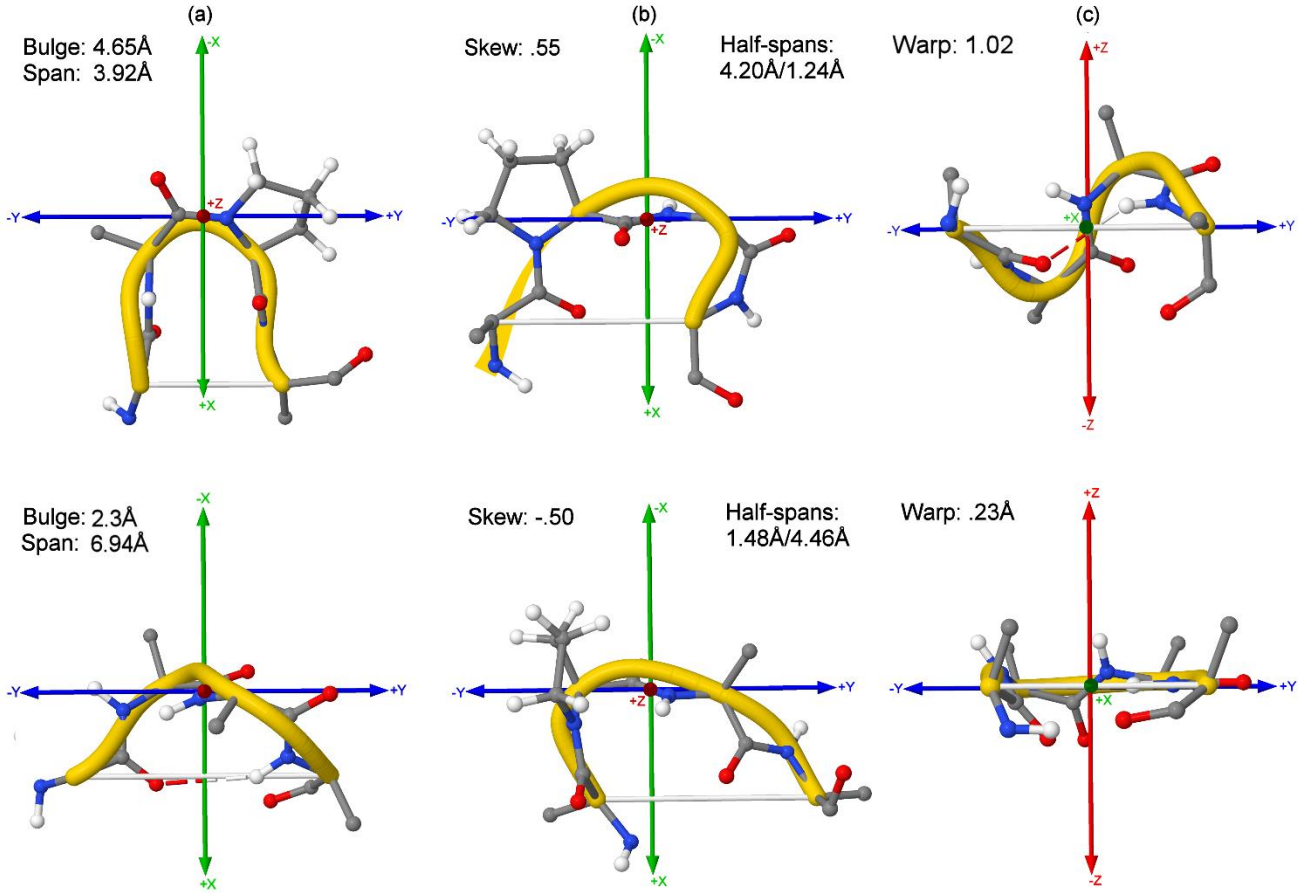

Figure 1. Parameter ranges in structures. Examples of turns that show parameter values near their limits in the dataset. To view any structure in ExploreTurns, load the entire database by clicking ***Load Turns Matching Criteria*** without any selection criteria, copy the PDB address into the ***PDB address*** box, and click ***Browse Structures***. The extent of the structure external to a turn that is displayed in the viewer is controlled with the ***Radius*** box; click ***Browse Structures*** again after entering a new radius. Note that while extreme parameter values are correlated with an increased frequency of geometric criteria with outliers in PDB validation checks (section 2.3 in Supplementary Material), none of these examples show outliers. **(a)** 5HKQ_I_74 (top) and 4YZZ_A_239 (bottom) represent the ranges of both bulge and span, since the two parameters exhibit very strong negative correlation (section 2.2 in Supplementary Material). **(b)** 5TEE_A_23 (top), and 3NSW_A_44 (bottom) represent strong positive (C-terminal) and negative (N-terminal) skew. Half-spans are also given. **(c)** 5BV8_A_1285 (top) and 3S9D_B_117 (bottom) represent the limits of warp in classical type I, and demonstrate the wide warp range that occurs within this type (and its associated BB cluster, AD_1).

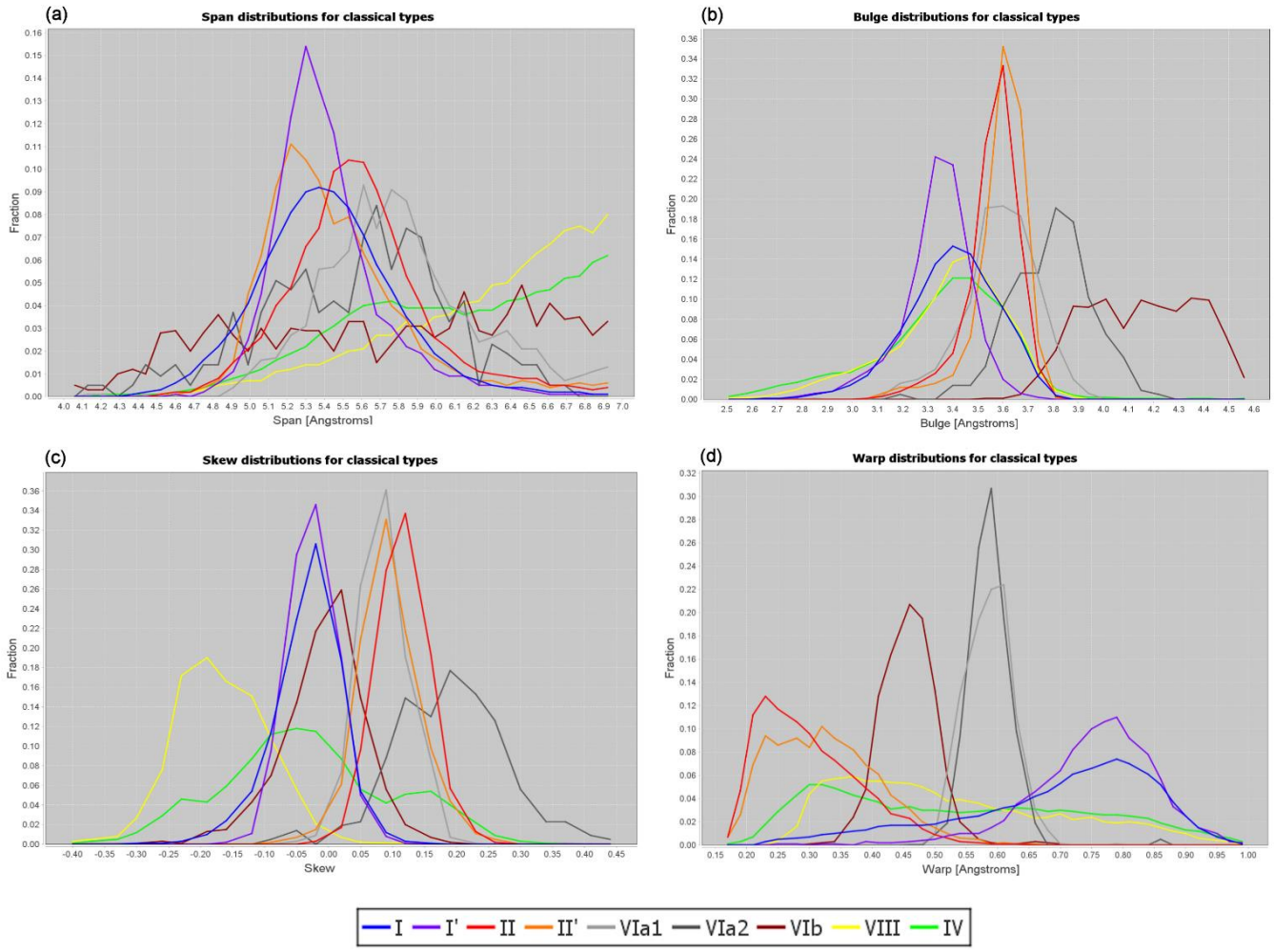

Figure 2. Distributions of the geometric parameters in the classical turn types. (a) Span: the type I' distribution (purple) peaks sharply near 5.3Å, reflecting its common role as a chain-reverser in 2:2 beta hairpins and contrasting with the broader peak of the type I distribution (blue), which is consistent with the wider range of type I roles. Types IV (structurally unclassified), VIb and VIII (green, brown, yellow) all show substantial abundance out to the 7Å limit of span, likely reflecting the scarcity of the constraining 4>1 H-bond in these types. **(b)** Bulge: types VIa2 and VIb (dark grey, brown) extend well to the right of all other types, while the modes for types II/II' fall to the right of those for types I/I'. All bulge distributions exhibit negative Pearson skewness[14], with more substantial tails on the left, indicating that the upper limit of bulge is "harder" than its lower limit: high-bulge/low-span (tighter) turns are more likely to be associated with conformational strain and steric clashes within the turn than low bulge/high span turns. **(c)** Skew: types (I, I', VIb) and (II, II', VIa1) can be formed into two loose groups that peak near skew 0 and .1 respectively, while types VIII and VIa2 peak to the left and right of these groups, and type IV covers the range of all structurally classified types. **(d)** Warp: the warp distributions form five groups from left to right, consisting of types (II, II'), (IV, VIII), VIb alone, (VIa1, VIa2), and (I, I'). Groups (II, II') and (IV, VIII) exhibit positive Pearson skewness, with long tails to the right, while (I, I') shows negative skewness. The similarity between the type IV and VIII distributions in span, bulge, and warp is notable.

3.3 Ramachandran-space parameter heatmaps

The distributions of geometric parameter values across the Ramachandran spaces of the backbone dihedral angles of the two central turn residues reveal the bond rotations that drive parameter variation. Figure 3 displays six examples of heatmaps of these distributions in the classical turn types or BB clusters; see the figure caption for interpretations. The ExploreTurns tool gives access to Ramachandran-space heatmaps for all parameters across all types, BB clusters and the global turn set.

3.4 H-bond energy vs. parameter value

Figure 4 plots the electrostatic (dipole-dipole) energy of the 4>1 BB H-bond versus geometric parameter values for classical types I and II, the largest types in which the H-bond is common. In type I, energy drops steadily with increasing warp, from .3 kcal/mol for the flattest turns to -1.8 kcal/mol at high warp (Figure 4a), while in type II energy shows a gradual increase as warp rises (Figure 4b). The negative correlation (r = -.61) between H-bond energy and warp in type I can be rationalized by the observation that the 4>1 H-bond donor and acceptor typically show a much poorer alignment, with a greater H…0 distance, in flatter vs. higher-warp turns due to rotations of the first and third peptide bond planes as warp falls; the primary factor is likely the rotation of the $C_1 \rightarrow O_1$ H-bond acceptor towards -z, but the $N_4 \rightarrow H$ donor can also rotate, towards +z. The incompatibility between low warp and the 4>1 H-bond in type I turns is a major contributor to the much lower frequency of this H-bond in type I (71%) than in the other three largest classical types that commonly exhibit it: I' (95%), II (86%), and II' (92%); H-bond frequency in the 47% of type I turns with warp greater than .75 is 90%.

In type I, energy falls as span increases until a minimum is reached near span 5.4Å, but then reverses its trend and rises steadily (Figure 4c), while in type II energy remains at its minimum as span increases until about 5.4Å, then rises steadily (Figure 4d). The rise in H-bond energy above 5.4Å in both types can be rationalized by the expected increase in H-bond length with increasing span, but the initial energy drop with rising span in type I defies this; it is likely best explained by the correlation between span and warp in this type (section 2.2 in Supplementary Material): lower span is associated with lower warp, which disrupts the H-bond.

H-bond energy is only weakly sensitive to skew in type II (Figure 4f), with low energy across the skew range, but in type I (Figure 4e) energy has its minumum at skew zero and rises dramatically with absolute skew.

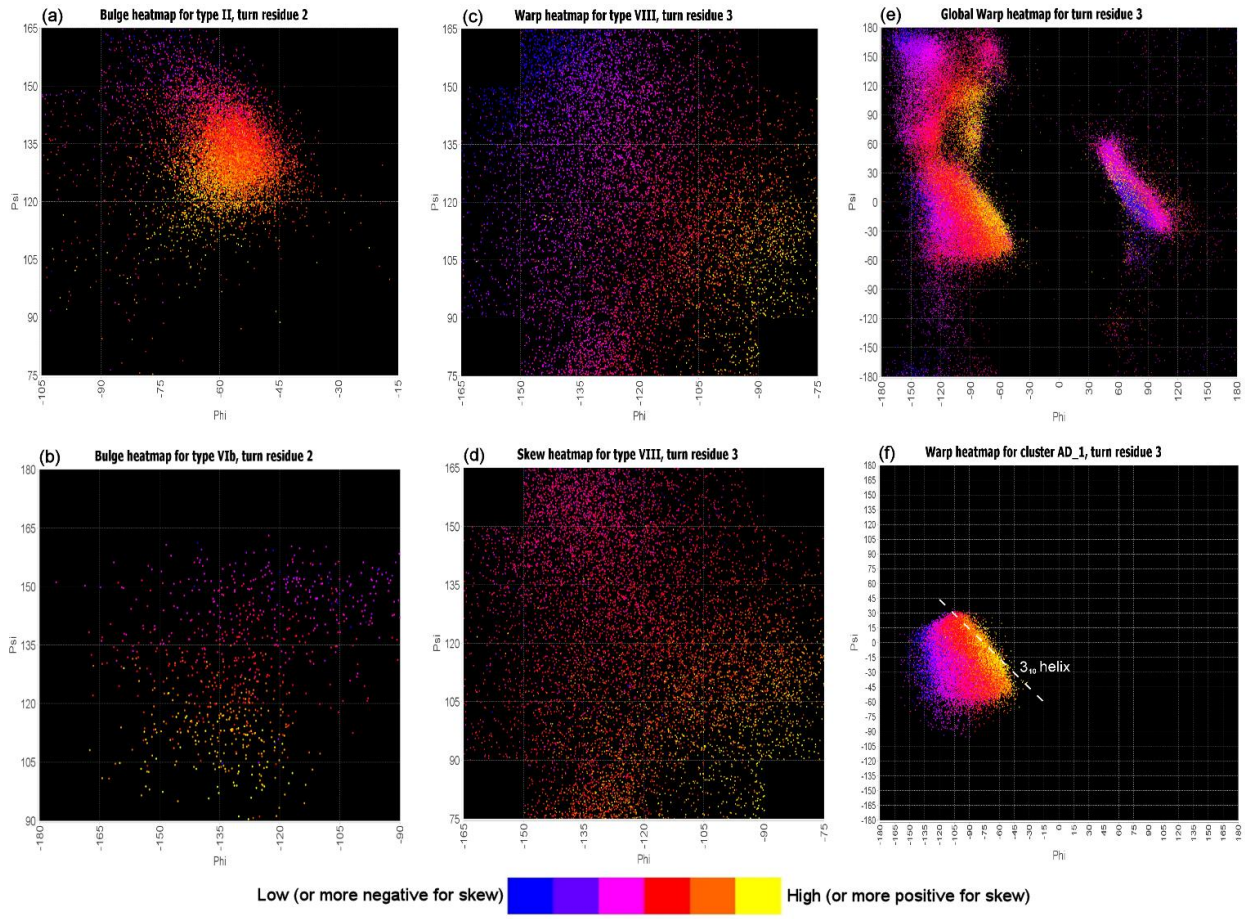

Figure 3. Ramachandran-space heatmaps reveal the bond rotations that drive parameter variation. Parameter values are colored on relative scales within each plot according to the legend; actual values can be obtained from ExploreTurns. **(a)** At the second residue of type II turns, rising ψ_2 reduces bulge by rotating $C_{\alpha 2}$→N_2 "outwards and upwards" (towards -y, +z), effectively reducing the x components of the three main-chain path bonds in the plane of the first peptide bond. **(b)** The second residue of type VIb turns shows a more uniform gradient of falling bulge as ψ_2 rises, driven by an almost directly outwards rotation of $C_{\alpha 2}$→N_2. **(c, d)** The warp and skew maps for residue 3 in type VIII turns show broad, highly correlated gradients of falling warp and increasingly negative skew from lower-right to upper-left as the residue opens into a more extended conformation, both flattening the turn and lengthening its C-terminal half-span. **(e)** The most characteristic feature of high-warp turns is the orientation of the second peptide bond approximately parallel to the z axis, and the global warp distribution at residue 3 shows a falling gradient over a wide range of ψ_3 as φ_3 becomes increasingly obtuse below -60° and the peptide bond rotates down towards the turn plane. **(f)** In the type I-associated cluster AD_1, which contains about half of all turns, warp rises as φ_3 becomes increasingly positive (more acute), supporting the sharper BB reversals required at $C_{\alpha 3}$to direct the BB back down towards the turn plane after the large z-dimensional excursions associated with high warp. Warp is maximal near the line along which (φ, ψ) sums to -75°, ideal for a 3_{10} helix, demonstrating the relationship between warp and helical character; a 3_{10}helix can be viewed as an extension of a (high-warp) beta turn[15].

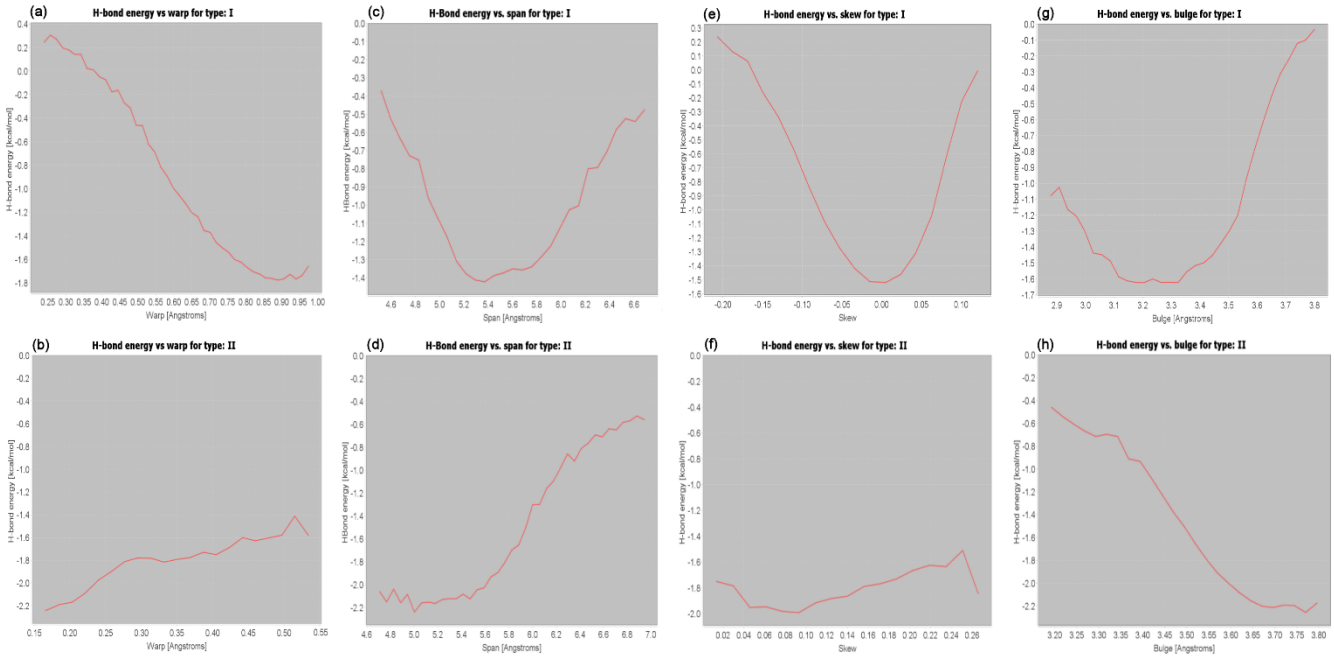

Figure 4. Electrostatic (dipole-dipole) energy of the 4>1 beta-turn H-bond vs. parameter value for span, bulge, skew and warp in classical types I and II. (a, b) Energy rises steeply with falling warp in type I, reflecting conformational changes that disrupt the H-bond as the turn flattens. By contrast, energy falls gradually with falling warp in type II. **(c, d)** Energy rises as span rises above 5.4Å in both types, but in type I energy also rises as span falls below 5.3Å, reflecting an association between low span and low warp (which disrupts the H-bond). **(e, f)** Energy shows only a weak dependence on skew in type II, but rises strongly with absolute skew in type I. **(g, h)** Energy falls steadily with increasing bulge in type II, in agreement with a simple wire-frame model in which span falls as bulge rises, but in type I energy increases as bulge climbs above 3.3Å, reflecting an H-bond-disrupting drop in warp with increasing bulge.

The steady drop in H-bond energy in type II as bulge increases (Figure 4h) can be explained as an indirect effect, operating through the negative correlation between bulge and span, that is consistent with the behavior of a simple wire-frame model for the turn: a larger bulge results in a smaller span, which shortens and strengthens the H-bond. However, this picture does not hold in type I (Figure 4g), where energy falls to a minimum near 3.2Å, then begins a steady rise from 3.3Å upwards. This behavior can also be rationalized as an indirect effect, this time operating through a strong negative correlation between bulge and warp in this type (r = -.77): rising bulge, like falling span, is associated with falling warp, which disrupts the H-bond.

3.5 Parameter dependence of sequence motifs

The overrepresentation of multiple key sequence motifs in beta turns and their BB neighborhoods shows clear dependencies on parameter values. Figures 5, 6 and 7 present plots of fractional overrepresentation vs. span, bulge, skew and warp for twelve sequence motifs which commonly form SC/BB H-bonds (Figures 5, 6), SC/SC H-bonds (Figure 7a,b), or pi-stacking interactions (Figure 7c); see the figure captions for discussion. As the plots show, turn parameters can serve as structural discriminators within classical types (or BB clusters) that dramatically increase the specificity and accuracy of measurements of sequence preferences in turns and their BB neighborhoods. For example, while the sequence motif that specifies Thr at turn position 3 (T3) is overrepresented by 48% in the set of all type I turns, Figure 6e shows that its overrepresentation peaks near 320% at low warp, reflecting its H-bonding role in the type 2 beta-bulge loop (BBL2).

With the guidance of built-in overrepresentation plots like those shown here, turn parameters can be used in ExploreTurns to select structures tuned for compatibility with particular sequence motifs, and the MapTurns tool comprehensively maps the BB and SC structures, H-bonding and contexts associated with these motifs.

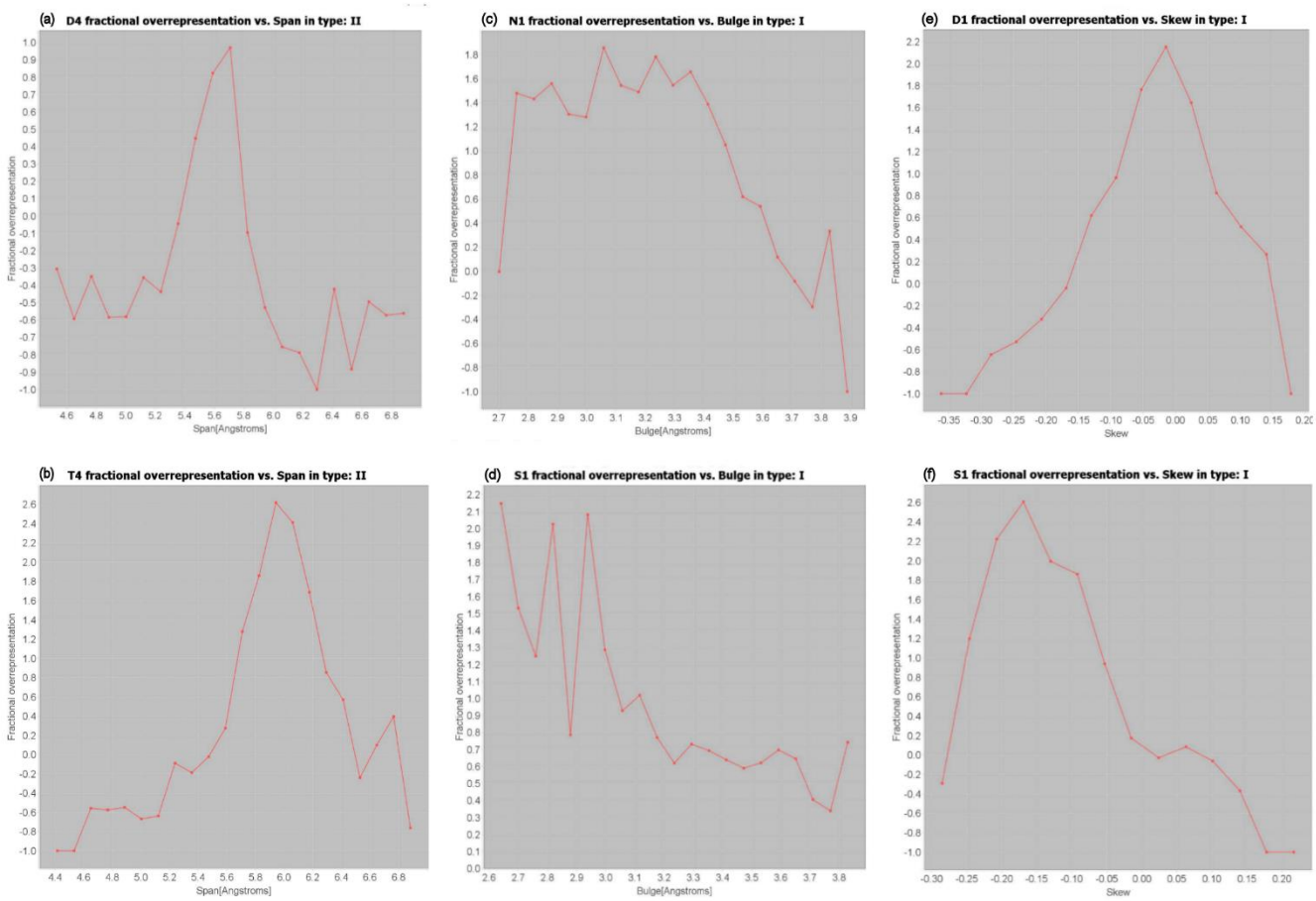

Figure 5. Examples of span, bulge and skew dependence of SC motifs. (a, b) Plots of the fractional overrepresentations of Asp and Thr at turn position 4 (D4 and T4) vs. span in type II turns show prominent maxima that likely correspond to the optimal spans for SC/BB H-bonding with the main-chain NH group of the first turn residue (MCN1, for D4) or the main-chain carbonyl group of that residue (MCO1, for T4). **(c, d)** The overrepresentation of Asn and Ser at turn position 1 in type I turns falls off with increasing bulge, which can be rationalized by the lengthening and weakening of the H-bond between these SCs (which participate in Asx/ST turns/motifs[16,17]) and MCN3 as bulge rises; S1's earlier falloff is consistent with its shorter SC. **(e, f)** While Asp at position 1 (D1) in type I turns shows peak overrepresentation near zero skew, Ser at position 1 (S1) shows a negative-skew bias, which can be rationalized by the suitability of a short N-terminal half-span for optimal H-bonding between Ser's shorter SC and MCN3.

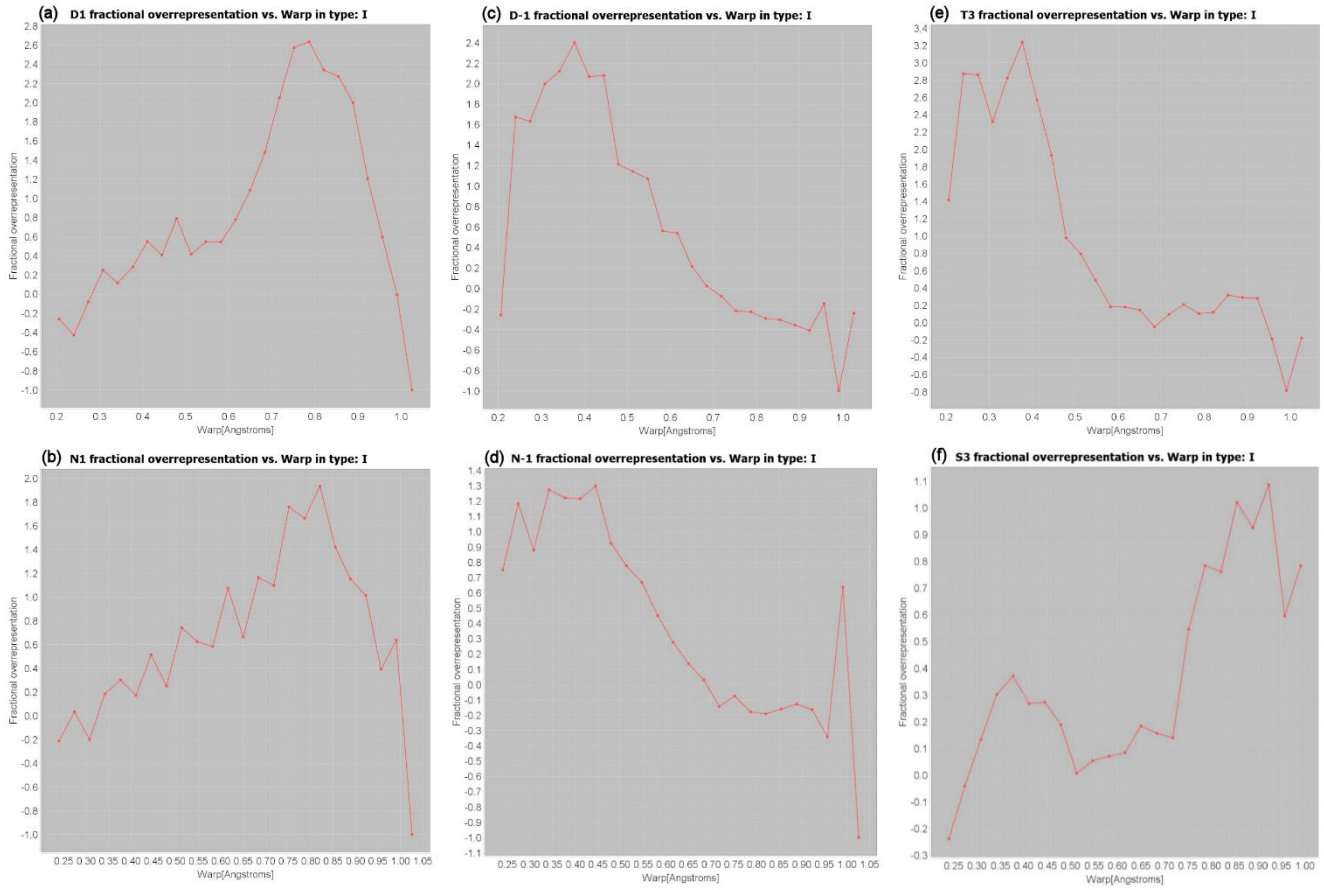

Figure 6. Examples of warp dependence of SC motifs. (a, b) Asp and Asn at turn position 1 (D1 and N1) in type I turns show peak overrepresentation at high warp, reflecting the compatibility of this geometry with SC/BB H-bonding in Asx turns/motifs[16], in multiple contexts including the type 1 beta-bulge loop[5,18] (BBL1) (see Figure 9g). **(c, d)** Asp and Asn just before the turn (D-1 and N-1) peak at low warp, reflecting compatibility with structures such as the type 2 beta-bulge loop[5,18] (BBL2, Figure 9h) and the alpha-beta loop[19], in which flatter turns orient at approximately 90° to the incoming BB; Asp/Asn SCs support these "upright turns" by H-bonding with MCN2/MCN3. **(e)** Thr at turn position 3 (T3) peaks at low warp, reflecting its roles in contexts including BBL2s, where its SC H-bonds with MCN+1, linking the loop's upright turn to its bulge (Figure 9h). **(f)** Ser at turn position 3 (S3) shows a low-warp peak, reflecting a role like that of T3 in BBL2s, as well as a high warp peak, reflecting roles including SC/SC H-bonding with D1 and SC/BB H-bonding with the bulge in BBL1s.

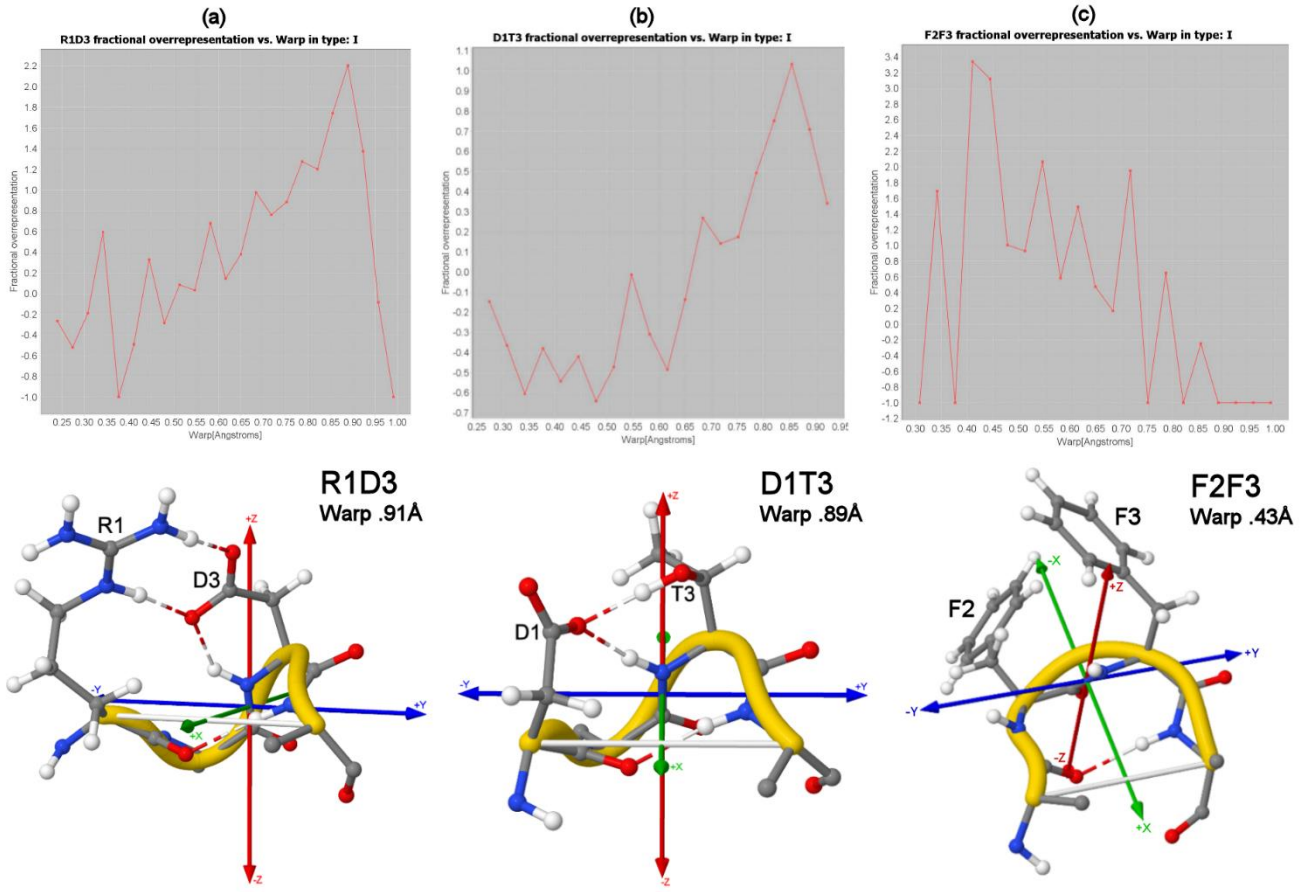

Figure 7. Examples of warp dependence of pair SC motifs. (a, b) Arg1+Asp3 (R1D3) and Asp1+Thr3 (D1T3) show strong preferences for high warp, which likely optimizes their SC positions for H-bonding (4A56_A_55 and 3AL2_A_1301). **(c)**: Phe2+Phe3 (F2F3) favors lower warp, which brings the SCs closer for perpendicular pi-stacking (3PYC_A_29).

3.6 Effect of *cis*-peptide bonds on bulge and skew

Figure 8 demonstrates strong relationships between the occurrence of *cis* conformations at the three peptide bonds in a beta turn and its skew and bulge, and these effects show a degree of superposition when *cis* conformations are combined (see the figure caption for details).

The skew biases of *cis*-peptide bonds can be compounded by combination with biased Ramachandran types. For example, the combination of a *cis* conformation at the first peptide bond (*cis1*, avg. skew -.18) with the negatively-biased type AB (-.25), yields *cis*AB (-.41), and the combinations of cis_3 (.16) with Ba (.20) yields Ba*cis* (.36), in which the biases add exactly. The Ramachandran type that specifies *cis*-Pro at both central turn positions (*cis*P*cis*P) shows extreme skew bias (-.46). To view a Ramachandran-region map in ExploreTurns, click ***Ramachandran Types***; turns of a particular type can be browsed by entering the type name in the ***Type or BB cluster*** box.

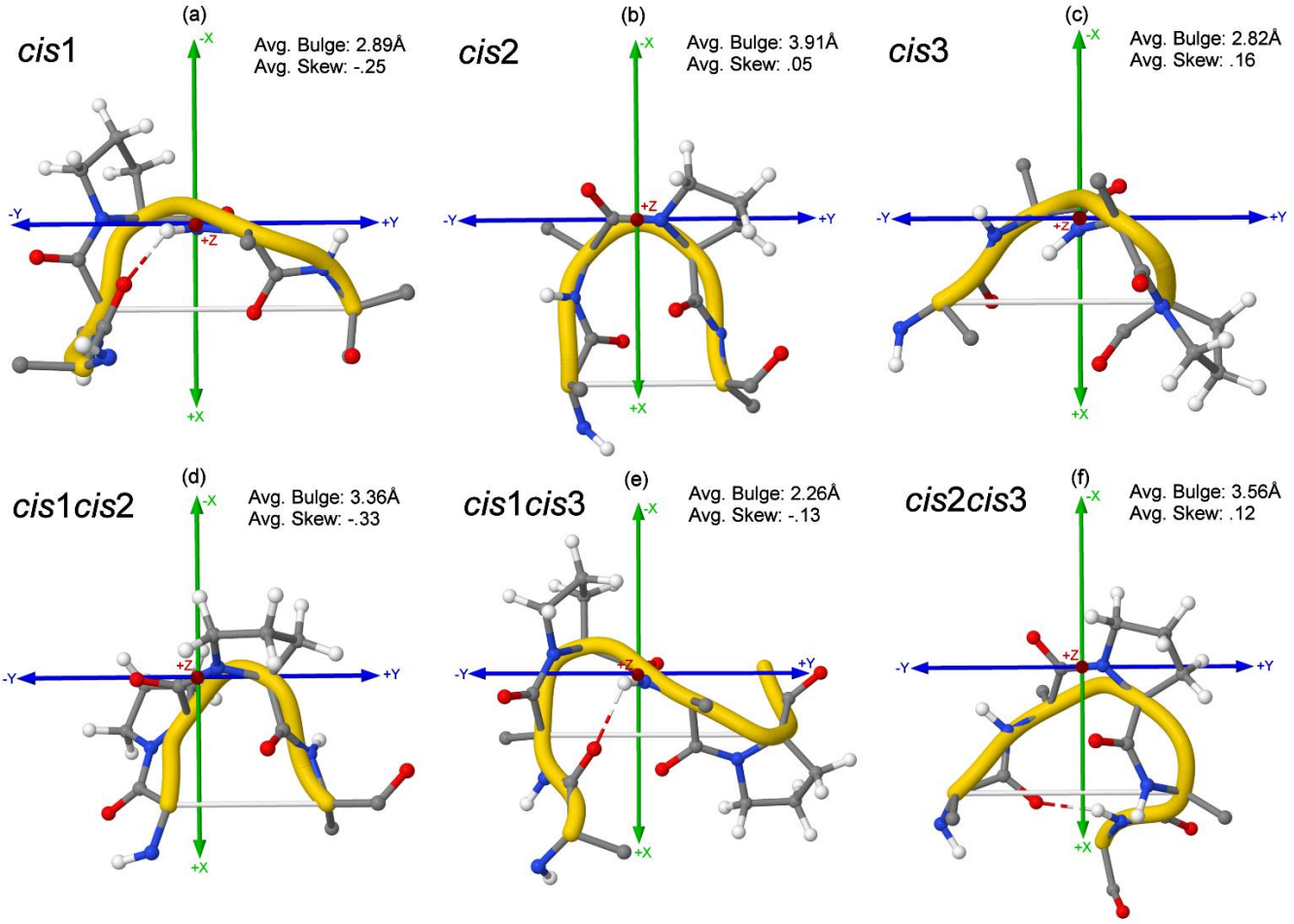

Figure 8. *cis*-peptide bonds influence bulge/skew and show a degree of superposition. (a) Turns with a *cis* conformation at the first peptide bond (cis_1) exhibit low average bulge (2.89Å vs. the 3.45Å global avg.) and a negative-skew bias (3O4P_A_140). **(b)** cis_2 turns show high bulge with a minor positive-skew bias (1SG6_A_99). **(c)** cis_3 turns show low bulge and a positive skew bias (3UCP_A_685). **(d, f)** In cis_1cis_2 and cis_2cis_3 turns, the low-bulge biases of the component cis_1 and cis_3 peptide bonds effectively cancel the high-bulge bias of cis_2, yielding bulges that straddle the global mean, while skew biases of the same signs as the cis_1 and cis_3 components persist (enhanced in cis_1cis_2) when combined with cis_2's near-neutral skew (3LCC_A_180, 4OW5_A_102). **(e)** In cis_1cis_3 turns, the low-bulge biases of the components show an additive effect, resulting in extreme low bulge, while cis_1's larger negative-skew bias is reduced by combination with cis_3's smaller positive bias (1ZR6_A_397).

3.7 Parameter correlations

The structural constraints imposed by bond lengths and angles in the beta-turn BB impose relationships between the geometric parameters, rendering them far from independent. Section 2.2 in Supplementary Material presents a table of parameter cross-correlations and rationalizes several key examples.

3.8 Roles of parameter variation

Turn parameters describe geometric variations which effect the roles and contexts of beta turns. The highly anti-correlated bulge and span parameters are of course major determinants of a turn's curvature, and turns of high bulge/low span are found where the BB must reverse within spaces that are narrow in the y dimension of turn coordinates. Bulge provides a degree of freedom in the x dimension of turn coordinates; turns with higher bulge project the BB and SC groups of a turn's central residues further toward -x to support structural interactions, participation in ligand binding or active sites, or increased solvent exposure. On the opposite end of the bulge/span scale, the most common context for turns with the largest spans is extended loops.

Skew is a measure of a turn's asymmetry in the y dimension, while the half-spans that determine skew represent degrees of freedom in this dimension that provide some independence in the positioning of BB and SC groups on each side of the turn axis, which can be used to satisfy packing constraints or support interactions. Ramachandran types which specify a more extended conformation at one central turn residue are associated with skew biases, since they lengthen one half-span. For example, Ramachandran types AB, AZ and AP show negative-skew biases due to their {B, Z, P} components; types AB and AZ are largely responsible for the negative skew bias of classical type VIII. Types Ba, Za, Pa and Pd show positive-skew biases, and Pa and Pd are responsible for most of classical type II's positive bias.

Warp describes BB excursions above and below the turn plane which can accommodate tight packing in the z dimension (low warp) or enable a turn's BB and SC groups to interact with structures farther above and/or below the plane (high warp).

Just as the values of all four parameters show particular regimes that are compatible with key SC motifs, they also exhibit compatibilities with the structures in a protein that incorporate turns, including beta sheets, local H-bonded motifs[19] and ligand-binding sites, and these structures influence turn geometry (affecting both parameter values and turn type) via H-bonding, covalent bonding, and/or stress communicated through the BB. Figure 9 displays eight examples of structural contexts for turns which are compatible with parameter values well above and below their global averages.

The 2:4 beta-hairpin[20] (Figure 9f) demonstrates a notable relationship between warp and beta-turn context. Most chain-reversing turns in 2:2 hairpins (the most common hairpin type) are of types I' or II'; turns of type I are much less common due to a geometric clash between the right-handed inter-strand twist of the hairpin's ladder

component and the left-handed twist between the turn's incoming and outgoing BB segments[21]. Low warp reduces this clash, rendering the turn more compatible with the ladder, but the conformational changes associated with warp reduction commonly disrupt the turn's 4>1 H-bond (Figure 4a), yielding a 2:4 hairpin in place of the more common 2:2 type. As a result, more than half of 2:4 hairpins in the dataset incorporate type I chain-reversing turns with below-average warp for the type, suggesting that a majority of 2:4 hairpins owe their existence to the compatibility between low warp and the ladder's twist.

The chain-reversing turns in type 1 and 2 BBLs, which are both commonly of type I, demonstrate another relationship between warp and context in beta turns. In the BBL1 (Figure 9g), a high-warp turn supports the loop's 4>1 H-bond, commonly forming the back of a "reclined chair", while in the BBL2 (Figure 9h), a low-warp geometry suppresses the 4>1 H-bond in favor of the 4>-1 alternative characteristic of the loop, and it is required for the loop's "upright chair" conformation.

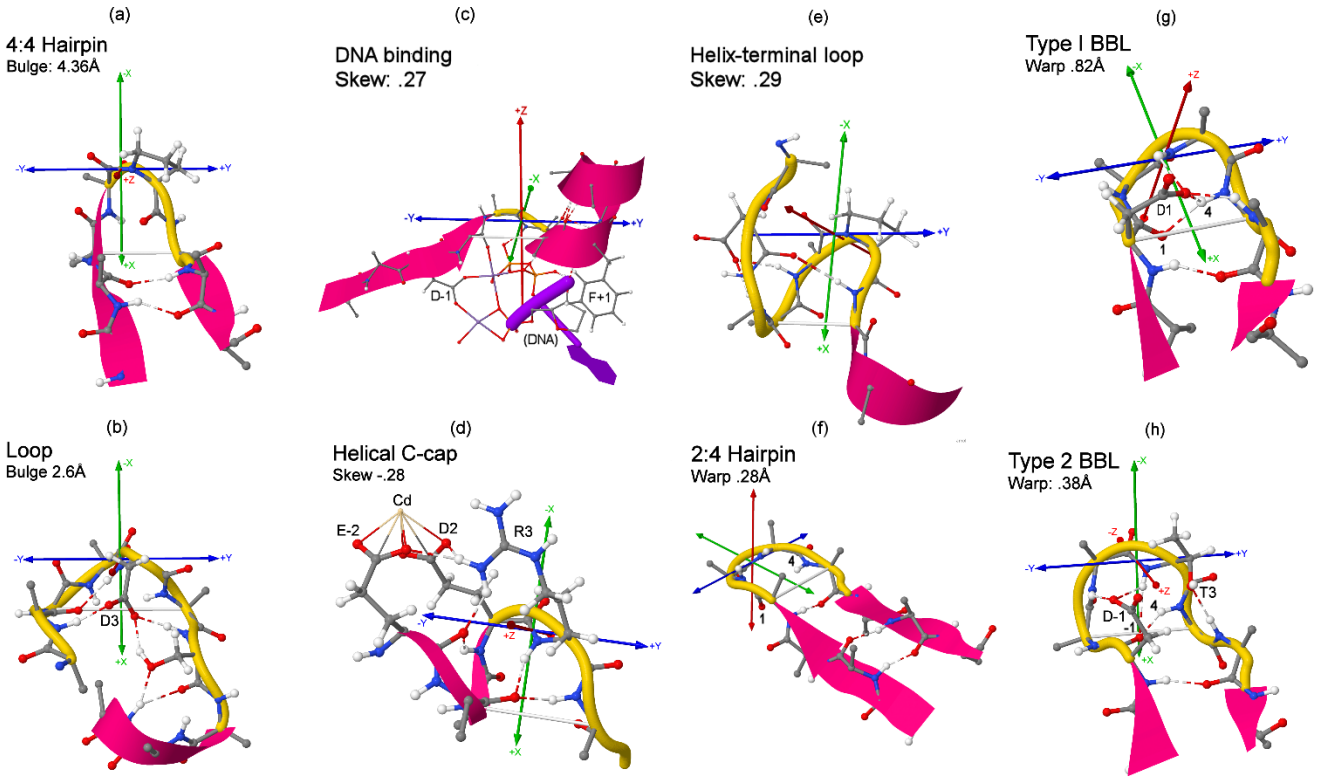

Figure 9. Examples of the structural roles of parameter variation. (a): Chain-reversing loops in 4:4 beta hairpins are commonly formed of high-bulge type VIb (mostly B*cis*P) turns (3AKS_A_81). **(b)**: The low bulge (and high warp) of a type IV (dA) turn in a helix-entrance loop positions the Asp SC at turn position 3 (D3) to mediate a network of H-bonds binding the loop (5UJ6_A_542). **(c)**: The positive-skew geometry of a type IV (Ba) turn in a strand-helix junction positions turn and helix groups for DTP/DNA binding in DNA polymerase (5KFZ_A_14). **(d)** The shorter N-terminal half-span of a negatively-skewed turn positions the helix for C-capping and Cd binding (3B40_A_50). **(e)** The short C-terminal half-span of a positively-skewed type VIa2 (B*cis*A) turn (avg. skew .25) is compatible with a BB H-bond that secures the geometry of a helix-terminal loop (3V5C_A_287). **(f)** The low warp of a type I turn simultaneously enables compatibility with the ladder component of a hairpin and disrupts the turn's 4>1 H-bond, yielding a 2:4 hairpin in place of the more common 2:2 type. **(g)** A high-warp type I turn is compatible with the BBL1's interior 4>1 BB H-bond, and it forms the back of the loop's "reclined chair". The motif is shown here with Asp at position 1 (D1, see Figure 6a) (4K9Z_A_34). **(h)** A low-warp type I turn is compatible with the "upright chair" conformation of a BBL2 along with its interior 4>-1 H-bond. The loop is shown with its chair-back turn supported by SC/BB H-bonds mediated by Asp just before the turn and Thr at turn position 3 (D-1 and T3, see Figure 6c,e) (3SCY_A_360).

3.9 Parameters and structure quality

Since geometric parameters enhance the description of turn geometry in Euclidean space, they may aid the detection and characterization of structurally suspicious conformations. Section 2.3 in Supplementary Material investigates the relationship between parameter values and structure quality and finds that extreme values are often associated with an increased frequency of geometric quality criteria with outliers as measured by PDB validation tools[22].

4 Discussion

The turn-local coordinate system and global alignment derived here resolve the difficulties with visualization inherent in the Ramachandran-space turn representation, providing a natural framework for the comparison and analysis of the wide variety of turn structures and the recurrent contexts in which they occur, including H-bonded motifs, supersecondary structures and ligand-binding sites.

Geometric parameters provide a Euclidean-space description of the bulk BB shapes of turns that reflects meaningful modes of geometric variation not explicitly captured by Ramachandran-space representations. Parameters complement existing turn classification systems, enabling a fine-tuning of backbone geometry within classical types or BB clusters which supports the selection of structures for compatibility with particular SC interactions and turn contexts, and produces major improvements in the specificity and accuracy of measurements of AA sequence preferences in turns and their BB neighborhoods.

Turn-local coordinates and geometric parameters should prove useful in any application where an enhanced Euclidean-space picture of turn structure can improve understanding or performance. One promising area of application is protein design, and in particular the design of binding and active sites, where turns are common and even small changes in geometry may have major impacts on function. Parameters may also prove useful in structure validation, by improving the characterization of suspicious conformations and identifying extreme geometries that may not always be highlighted as outliers by existing validation tools.

Declarations

Availability of data and materials

All data supporting the conclusions of this article are available from the Protein Data Bank at www.rcsb.org. The ExploreTurns, MapTurns and ProfileTurn web tools are available at www.betaturn.com.

Competing interests

The author declares that he has no competing interests.

Funding

This work was funded entirely by the author.

Acknowledgements

The author wishes to thank Athena Newell for useful discussions and work as a research assistant and Kit Newell for work as a research assistant. The constructive suggestions and support of the attendees of ISMB/3DSig 2019 (Basel) and the 33rd and 37th annual symposia of The Protein Society (2019 Seattle and 2023 Boston) also contributed to the development of this project.

Supplementary Material

Supplementary file 1 (PDF)**.** Supplementary sections.

References

1) Koch O, Klebe G. Turns revisited: A uniform and comprehensive classification of normal, open, and reverse turn families minimizing unassigned random chain portions. *Proteins*. 2009;74(2):353-67.

2) Isogai Y, Némethy G, Rackovsky S, Leach SJ, Scheraga HA. Characterization of multiple bends in proteins. *Biopolymers*. 1980;19(6):1183-210.

3) Venkatachalam CM. Stereochemical Criteria for Polypeptides and Proteins. V. Conformation of a System of Three Linked Peptide Units. *Biopolymers*. 1968;6(10):1425-36.

4) Shapovalov M, Vucetic S, Dunbrack RL. A new clustering and nomenclature for beta turns derived from high-resolution protein structures. *PLOS Computational Biology*. 2019;15(3).

5) Newell, NE. ExploreTurns: A web tool for the exploration, analysis and retrieval of beta turns and their contexts in proteins; application to beta-bulge loops and helix capping. *bioRxiv.* doi: https://doi.org/10.1101/2024.01.01.573820

6) Hutchinson EG, Thornton JM. A revised set of potentials for β-turn formation in proteins. *Protein Science*. 1994;3(12):2207-16.

7) Hollingsworth SA, Karplus PA. A fresh look at the Ramachandran plot and the occurrence of standard structures in proteins. *Biomol Concepts*. 2010;1(3-4):271-83.

8) Hauser K, He Y, Garcia-Diaz M, Simmerling C, Coutsias E. Characterization of biomolecular helices and their complementarity using geometric analysis. *Journal of Chemical Information and Modeling*. 2017;57(4):864-74.

9) Newell, NE. MapTurns: mapping the structure, H-bonding and contexts of beta turns in proteins. *bioRxiv*. doi: https://doi.org/10.1101/2024.01.02.573949

10) Berman HM, WestBrook J, Feng Z, Gilliland G, Bhat TN et al. The Protein Data Bank. *Nucleic Acids Res*. 2000;28(1):235-242

11) Bishop YM, Fienberg SE, Holland PW. Discrete Multivariate Analysis: Theory and Practice. New York: Springer; 2007.

12) Hu JC, Newell NE, Tidor B, Sauer RT. Probing the roles of residues at the e and g positions of the GCN4 leucine zipper by combinatorial mutagenesis. *Protein Science*. 1993;2(7):1072-84.

13) Newell NE. Mapping side chain interactions at protein helix termini. *BMC Bioinformatics*. 2015;16:231.

14) Doane DP, Seward LE. Measuring skewness: A forgotten statistic? *Journal of Statistics Education*. 2011;19(2).

15) Pal L, Basu G, Chakrabarti P. Variants of 3(10)-helices in proteins. *Proteins*. 2002;48(3):571-9.

16) Wan W-Y, Milner-White EJ. A natural grouping of motifs with an aspartate or asparagine residue forming two hydrogen bonds to residues ahead in sequence: their occurrence at α-helical N termini and in other situations. *Journal of Molecular Biology*. 1999;286(5):1633-49.

17) Wan W-Y, Milner-White EJ. A recurring two-hydrogen-bond motif incorporating a serine or threonine residue is found both at α-helical N termini and in other situations. *Journal of Molecular Biology*. 1999;286(5):1651-62.

18) Milner-White EJ. Beta-bulges within loops as recurring features of protein structure. *Biochim Biophys Acta*. 1987;911(2):261-5.

19) Leader DP, Milner-White EJ. Motivated Proteins: A web application for studying small three-dimensional protein motifs. *BMC Bioinformatics*. 2009;10:60.

20) Sibanda BL, Thornton JM. Beta-hairpin families in globular proteins. *Nature*. 1985;316(6024):170-4.

21) Richardson JS. The anatomy and taxonomy of Protein structure. *Adv. Protein Chem*. 1981; 34:167-339.

22) Gore S, Garcia ES, Hendrickx PMS, Gutmanas A, Westbrook JD et al. Validation of Structures in the Protein Data Bank. *Structure*. 2017;25(12):1916-1927.